A sensitive method for determining UDP-Glucose: Ceramide glucosyltransferase (UGCG) activity in biological samples using deuterated glucosylceramide as acceptor substrate

Michele Dei Cas[1], Sara Casati[2], Gabriella Roda[3], Pablo Sardi[4], Rita Paroni[1], Alessio di Fonzo[5,6], Marco Trinchera[7]

[1] Department of Health Sciences, San Paolo Hospital, Università degli Studi di Milano, 20142, Milano, Italy

[2] Department of Biomedical, Surgical and Dental Sciences, Università degli Studi di Milano, 20133, Milan, Italy

[3] Department of Pharmaceutical Sciences, Università degli Studi di Milano, 20133, Milan, Italy

[4] Sanofi, Framingham, MA, United States

[5] Dino Ferrari Center, Neuroscience Section, Department of Pathophysiology and Transplantation, Università degli Studi di Milano, 20122, Milan, Italy

[6] Foundation IRCCS Ca' Granda Ospedale Maggiore Policlinico, Neurology Unit, 20122, Milan, Italy

[7] Department of Medicine and Surgery (DMC), University of Insubria, 21100, Varese, Italy

Corresponding author: Marco Trinchera, Dipartimento di Medicina e Chirurgia, Università dell'Insubria, via JH Dunant 5, 21100 Varese, Italy, email: marco.trinchera@uninsubria.it (to whom proofs and reprints should be addressed)

Running Title: UGCG activity assay

Key words: Ganglioside / Glycosphingolipid / Gaucher disease / Mass spectrometry

Abstract

Glucosylceramide synthase (UGCG) is a key enzyme in the biosynthesis of glycosphingolipids and its activity is related to the resistance to anticancer drugs and is involved in the derangement of metabolism in various diseases. Moreover, UGCG acts as a major controller of the balanced levels of individual brain sphingolipids that may trigger neurodegeneration in Gaucher disease and in Parkinson disease associated to pathogenic variants in the glucocerebrosidase-encoding gene *GBA*. We have developed an effective method for determining UGCG activity in vitro using deuterated ceramide as an acceptor, and quantitation of the formed deuterated glucosylceramide by liquid chromatography coupled with tandem mass spectrometry. The method enabled us to determine the kinetic parameters of UGGC and the effect of the inhibitor GZ667161 on the enzyme activity expressed in model cells, as well as to measure UGCG specific activity in human fibroblasts using a simple crude cell homogenate. This novel approach may be useful in determining the actual UGCG activity levels in patient cells and tissues of animal models of diseases, and to study novel drugs targeting glycosphingolipid metabolism.

Introduction

UGCG, UDP-Glucose: Ceramide β1-1' glucosyltransferase, EC:2.4.1.80, also known as glucosylceramide (GlcCer) synthase catalysed the reaction:

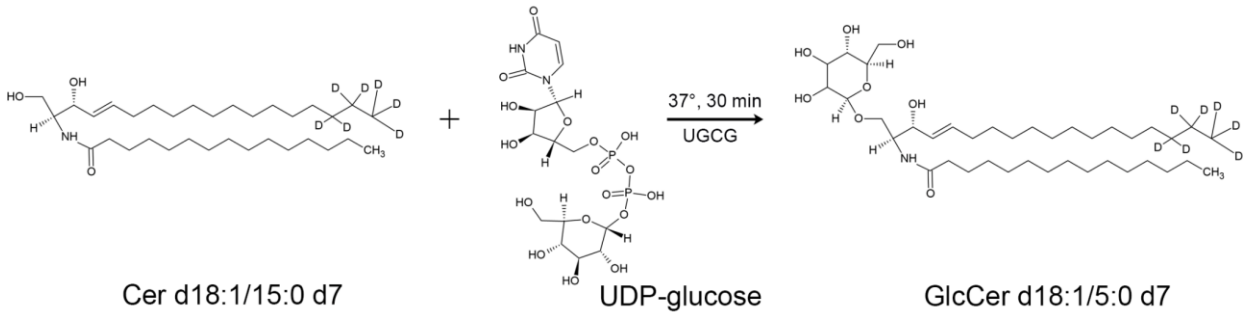

The enzyme responsible for the biosynthesis of the bulk of glycosphingolipids in mammals, since the reaction product, GlcCer, is the immediate precursor of lactosylceramide, the core structure common to almost all classes of complex glycosphingolipids, such as globosides, gangliosides and lacto- or neo-lacto neutral or sulfated glycosphingolipids (Belarbi et al., 2020). In addition to such a relevant physiologic role, UGCG merited special attention due to the involvement in drug resistance in various cancers (Wegner et al., 2018 a; b; Madigan et al., 2020; Salustiano et al., 2020; Bataller et al., 2021; Chueakwon et al., 2022), in the metabolic derangement occurring in malignant (Schömel et al., 2020; Jennemann et al., 2021; Zhang et al., 2021) and non-malignant diseases (Andersson et al., 2021; Baccam et al., 2022), and more recently, in the development of Parkinson disease (PD) in patients carrying mutations in the GBA gene (Sidransky et al., 2009). According to the hypothesis that reduced glucocerebrosidase activity gives rise to an imbalance between GlcCer and Cer that triggers α-synuclein accumulation and Parkinson disease (Riboldi et al., 2019; Belarbi et al., 2020), reducing GlcCer biosynthesis appeared a logical therapeutic approach that could be addressed inhibiting UGCG ubiquitously, mainly in the central nervous system. To this aim, potential inhibitors, including those able to pass the blood brain barrier, have been designed and tested in vivo and in vitro (Cabrera-Salazar et al., 2012; Marshall et al., 2016; Sardi et al., 2017; Fujii et al., 2021; Dodge et al., 2022; Sabnis, 2022; Tanaka et al., 2022). One of the main tools for addressing such issues is an assay for measuring UGCG activity in vitro. Between the assay methods reported so far (Roy et al., 2019), none concurrently overcomes the three main obstacles encountered since several years: a reliable enzyme source,

a suitable acceptor substrate not far from the natural one, and an accurate but convenient method for reaction product quantification. Taking advantage from our recent work with other glycosyltransferases (Indellicato et al., 2019, 2020), we have thought to bypass the first obstacle by obtaining relevant amounts of stable UGCG through transient over-expression in mammalian cells upon transfection of cDNA placed in an effective vector. Regarding the acceptor, we decided to incubate the enzyme with a commercially available isotope of Cer resembling the naturally occurring one: the deuterated C15-acyl-sphingosine. In the end, we detected and quantitate the formed deuterated GlcCer by LC-MS/MS of the reaction mixture. To test the efficacy of the procedure, we determined the GlcCer synthase specific activity in human skin fibroblasts, and evaluated the inhibitory effect of GZ667161 (Venglustat), a brain-penetrant clinical candidate GCS inhibitor already tested in a phase 2 clinical trial for *GBA*-PD, (Viel et al., 2021; Peterschmitt et al., 2022), on the enzyme activity.

Results and discussion

HEK-293T cells, which are efficiently transfected with plasmid DNAs and able to replicate plasmids carrying the Polyoma origin of replication, were found expressing extremely low levels of UGCG transcript, about 10^4-fold less than the housekeeping GAPDH. On the other hand, upon transfection of pCDNA3-UGCG, the transcript levels rose in HEK-293T (HEK-UGCG) to the same levels as GAPDH (Fig 1 panel A), a very promising value for further detection of enzyme activity. Previously, cell clones made able to stably express UGCG were used as enzyme source, but the levels of overexpression reported was much lower (Crespo et al., 2008; Wegner et al., 2018 a) . For comparison, in human fibroblasts the UGCG transcript levels were about 5-fold more abundant than in HEK-293T. Consequently, we decided to use homogenate prepared from HEK-UGCG and mock transfected HEK-293T cells as the positive and negative enzyme source, respectively, for setting detection of GlcCer synthase activity. In such preliminary experiments, we also set conditions for Cer solubilization and found that 5 mg/ml of Triton-X100 are enough for solubilizing up to 5 μM Cer, without interfering with LC-MS/MS analysis.

The LC-MS/MS analysis of samples (Fig. 2) coming from HEK-UGCG, mock transfected HEK-293T or human skin fibroblasts was able to simultaneously characterize and quantify both the enzymatic product (GlcCerd7, Fig. 2 panels A, C, and E) and the substrate (Cerd7, panels B and D). The use of deuterated compounds was necessary for being distinguishable, in their molecular masses, from endogenous sphingolipids, which can interfere with the analysis and overestimate UGCG activity.

Under the reaction conditions established, a peak corresponding to GlcCerd7 was detected by LC-MS/MS in the reaction mixture containing pcDNA3-UGCG transfected HEK-293T cells that appeared virtually absent with mock transfected cells. For evaluating the UGCG activity of skin fibroblasts (Fig. 1 panels B and C), the use of a high-sensitivity mass spectrometer was necessary due to the much lower endogenous activity present in primary cells with respect to transfected model cells.

The amount of GlcCerd7 formed and assumed as the measure of UGCG activity was found linear with time up to 20 min, and with homogenate protein concentrations ranging 1-4 mg/ml, corresponding to 20-80 μg per assay performed in a final volume of 20 μl (Fig. 1 panels B and C). The activity was strongly inhibited by addition of manganese ions that should be avoided (Supplementary Fig. 1, panel A). Other methods using either NBD-Cer (Ichikawa et al., 1996; Hayashi et al., 2005) or C8-Cer (Fu et al., 2019; Fujii et al., 2021) as acceptors avoided manganese ions or even added EDTA to the reaction mixture. Incubations lasted one hour or longer, but an actual comparison is not possible because shorter reaction times were not systematically tested. At constant saturating Cerd7 concentration (60 μM), under identical conditions, the activity was saturated at very hight UDP-Glc concentrations (over 12 mM,) with an apparent Km of 5.5 mM for UDP-Glc (Fig. 1 panel D). At constant saturating UDP-Glc concentration (15 mM) in the presence of 2 mg/ml HEK-UGCG homogenate, the activity was saturated at a Cerd7 concentration over 50 μM, with a calculated apparent Km 19.3 μM (Fig. 1 panel E). Noteworthy, kinetic parameters were different from those calculated using other assay methods, especially for UDP-Glc that was frequently added at concentrations ranging 0.2-0.5 mM (Ichikawa et al., 1996; Hayashi et al., 2005; Fu et al., 2019; Fujii et al., 2021), according to Km values reported to be 3-20 μM depending on the different sources (Crespo et al., 2008; Fujii et al., 2021). Due to such a relevant discrepancy, we have measured by LC-MS/MS the actual amounts of Cerd7 residual at the end of

the reaction, which were found higher than 90%. We also noticed that in the above reports the Km for UDP-Glc was calculated at substrate concentration much lower than 60 μM, being 20 μM for NBD-Cer (Crespo et al., 2008) or 7.4 μM for C8-Cer (Fujii et al., 2021). Moreover, the maximal UDP-Glc concentration tested was 0.4 (Crespo et al., 2008) or 0.1 mM (Fujii et al., 2021). Increasing UDP-Glc concentration not over 0.4 mM and using two non-saturating Cerd7 concentrations (20 and 5.0 μM), we also obtained much lower Km values: 182 and 53 μM, respectively (Supplementary Fig.1, panels A and B). This finding suggests that the differences in the Km values reported depend on the different assay conditions more than on the different assay methods. We also measured UGCG activity in the presence of various concentrations of GZ667161, an UGCG inhibitor recently investigated in a phase 2 clinical trial for *GBA*-PD patients, and found a robust inhibition over 5 μM (Fig. 1 panel F). Repeating the Cerd7 concentration curve in the presence of 10 μM GZ667161, we found that the apparent Km for Cer rises to 36.4 μM (less than 2-folds) while the apparent Vmax calculated with the same cell homogenate decreases almost 60-folds, from 35.9 to 0.60 pmol/mg*min (panel G). These data suggest a complex prevalently non-competitive inhibition mechanism by this drug. A relevant application of UGCG activity assay involves cells from patients potentially at risk for GlcCer imbalance due to reduced glucocerebrosidase activity. To this aim, we tried to evaluate UGCG activity in human fibroblasts. Taking into account the low UGCG transcript amounts expressed in these cells, we expected to find weak activity levels in fibroblasts, corresponding to minimal quantities of GlcCerd7 in the reaction mixture. We thus plan to use a more sensitive spectrometer able to detect less than 5 fmol of reaction product in the reaction tubes. An UGCG activity linear with time and homogenate protein concentration was detected in human neonatal skin fibroblasts and found similar to that found in transfected HEK-293T cells, but with a specific activity about 100-folds lower (Fig. 1 panels B and C, see the different scales used). In other fibroblasts, from human adults, UGCG activity values were found about 20% lower than in neonatal cells. HEK-293T cells transfected with the only pathogenic variant of UGCG reported (Monies et al., 2018) presented no activity over the background despite the high levels of the transcript (not shown). These data indicate that this novel approach may be useful in determining the actual UGCG levels in patient cells and in tissues of animal models of diseases because it is simple, reliable and requests to use simple crude

homogenates for quantitative assays. Without the discomforts and costs of manipulating radioactive substances, the proposed approach combines the advantages of an isotopically labeled natural substrate with a sensitivity similar or even better than that reported with non-physiologic C8-Cer or NBD-Cer. Moreover, it appears suitable for screening and characterizing new drugs affecting glycosphingolipid metabolism. We lack the equipment for the high throughput assay reported as fire MS (Fujii et al., 2021; Tanaka et al., 2022) but speculate that our method could be efficiently adapted to such an automated procedure. In the end, the use of transiently transfected HEK-293 cells allows quick and accurate comparison between wild type UGCG and variants potentially discovered in the future.

Materials and Methods

DNA constructs

Human UGCG cDNA was obtained by PCR using total RNA extracted from COLO-205 cells (Zulueta et al., 2014) using Phusion High-fidelity Taq polymerase (ThermoFischer Scientific), according to the manufacturer's protocol. The following primer pair was used: (forward) 5'-CGCG*GAATTC*ATGGCGCTGCTGGACCTGG and (reverse) 5'-CGCG*TCTAGA* TTATACATCTAGGATTTCCTCTGCTGTAC, containing EcoRI and XbaI restriction sites, respectively (italicized). Annealing was at 64°C, and 30 cycles of amplification were run. The obtained fragment was purified by spin columns, digested with EcoRI, re-purified, digested with XbaI, purified again, and ligated to pcDNA3 vector previously digested/purified with the same enzymes. A small aliquot of ligation reaction was used for transforming E. Coli Max-efficiency DH5α (ThermoFischer Scientific) and the obtained colonies used for inoculating a liquid culture to be used for preparing plasmid DNA. After assessing clones by restriction digestion, two of those potentially suitable were submitted to direct DNA sequencing.
pCDNA3-UGCG construct was mutagenized to insert an additional A using QuikChange II-E Site-Directed Mutagenesis Kit (Agilent Technologies) and the following primer pair (forward) 5'-CTGACAAACAGCCTTATAAGCAAGCTCCCAGGTGTC and (reverse)

5’GACACCTGGGAGCTTGCTTATAAGGCTGTTTGT CAG, designed to introduce the following variant in the UGCG sequence (NM_003358): c.142dupA; p.Ser48Lysfs*18 (Monies et al., 2018).

Cell culture, transfection, and processing.

HEK-293T cells were grown in DMEM supplemented with 10% fetal bovine serum and transiently transfected with plasmid DNA in the presence of Fugene-HD (Promega) as previously reported (Indellicato et al., 2020). Upon transfection, cells were harvested by trypsinization, pelleted, washed twice with PBS and aliquoted. A small aliquot (< 0.5 x 10^6 cells) was used for total RNA extraction using Relia-Prep RNA kit (Promega), another aliquot (about 2 x10^6 cells) was submitted to lipid extraction for LC-MS/MS analysis, and the remaining cells (2-10 x10^6 cells) were resuspended in 0.1 M Tris/HCl buffer, pH 7.5, containing 0.5% TritonX-100, vortexed to homogeneity, and stored in aliquots at -80°C. After thawing on ice, such crude homogenate was used as the enzyme source for in-vitro assay. Protein content was determined by the bicinconic acid method (BCA protein kit, ThermoFischer Scientific). Homogenate for enzyme assay were kept at protein concentration about 10-20 mg/ml.

Human neonatal (P10857) and adult (P10858) fibroblasts were purchased from Innoprot (Bizkaia, Spain) and cultured in DMEM supplemented with 10% foetal bovine serum and antibiotics. Cell harvesting and aliquot preparation were performed as for transfected HEK-293T cells.

Reverse transcription quantitative real-time polymerase chain reaction.

First strand cDNA was synthesized from 0.5-1 µg of total RNA by a commercial kit (GoScript oligodT mix, Promega). Control reactions were prepared by omitting the reverse transcriptase in the reaction. cDNAs were diluted 1:4, v/v, with mQ water and 1–2.0 µL of first strand reactions were amplified in a volume of 20 µL using Sybr Premix Ex Taq (Tli RNase H Plus, Takara), ROX as reference dye and StepOnePlus instrument (Applied Biosystem Life Technologies) as reported (Aronica et al., 2017). Primer sequences for UGCG amplification were as follows: (forward) 5’-GTGATAGTGGAATAAGAGTAATTCC, (reverse) 5’-

TGAAGTTCCAAAATATACCTGCTC. Annealing temperature was 60°C. The amounts of amplified target UGCG cDNA were calculated as ΔCt with respect to GAPDH (Aronica et al., 2017).

UGCG activity assay.

Cerd7 (deuterated C15-acyl-sphingosine, 860681 - C15 Ceramide-d7 [d18:1-d7/15:0], Avanti Polar Lipids), 20-400 pmol dissolved in chloroform/methanol, 2:1 (v/v) and 7.5 μg Triton-X100 in the same solvent were placed together at the bottom of 0.6 ml microcentrifuge tubes and allow to dry at RT under hood, and then kept at -20°C until used. A reaction solution was prepared and added to each tube in order to obtain the following final concentrations: 0.2 M Tris/HCl pH 7.0 and 15 mM UDP-Glc. In an ice-bucket, 10-40 μg of homogenate protein was added to each tube already containing water to a final volume of 10-20 μl. The reactions were started placing the tubes at 37°C, incubated for 10-30 min, and stopped by placing on ice and then stored at -20°C. GZ667161, 2 mM aqueous solution, was provided by Sanofi.

Reaction product characterization and quantification by LC-MS/MS.

UGCG activity reactions were precipitated by addition of pure methanol (75 μL) and centrifugated at 13400 rpm for 10 min. The precipitates were discharged and pure extracts (5 μL) were directly injected in LC-MS/MS. LC-MS/MS of extracts The extracts obtained from the reactions with transfected cells were consisted of a LC Dionex 3000 UltiMate (ThermoFisher Scientific, Waltham, MA, USA) coupled to a tandem mass spectrometer AB Sciex 3200 QTRAP (AB Sciex, Concord, Canada) equipped with electrospray ionization TurboIonSpray™ source operating in positive mode (ESI+). Chromatographic separation was carried out on a reverse-phase Acquity UPLC BEH C8 column 1.7 μm particle size, 100 × 2.1 mm (Waters, Franklin, MA, USA) at 30 °C using a linear gradient elution with two solvents: 0.2% formic acid and 2 mM ammonium formate in water (solvent A) and 0.2% formic acid and 1 mM ammonium formate in acetonitrile (solvent B). The chromatographic and mass spectrometry conditions can be found in detail in (Morano et al., 2022). The substrate (Cerd7) and the reaction product (GlcCerd7) were monitored by multiple reaction

monitoring as follows: Cerd7 (*m/z* 531.5>271.3, CE 30 eV, DP 45 eV) and GlcCerd7 (*m/z* 693.6>271.3, CE 45 eV, DP 45 eV). The extracts obtained from the reactions with skin fibroblasts were analyzed by a high-sensitivity LC-MS/MS consisted of QTrap 5500 triple quadrupole linear ion trap mass spectrometer (Sciex, Darmstadt, Germany) coupled with an Agilent 1200 Infinity pump Ultra High-Pressure Liquid Chromatography (UHPLC) system (Agilent Technologies, Palo Alto, CA, USA) using the same column and adapted chromatographic conditions reported in (Morano et al., 2022). The substrate (Cerd7) and the reaction product (GlcCerd7) were monitored by multiple reaction monitoring as follows: Cerd7 (*m/z* 531.5>271.3, CE 30 eV, DP 65 eV) and glucCerd7 (*m/z* 693.6>271.3, CE 45 eV, DP 65 eV).

Equations and statistical analysis

UGCG follows a classical Michaelis-Menten kinetic. For graphical description and kinetic constant calculations, the Hanes-Woolf equation was used: $[S]/v = 1/V_{max} * [S] + K_m/V_{max}$. Linear regression was obtained through Microsoft Excel. R^2 values were 0.982 (UDP-Glc saturation curve), 0.990 (Cerd7 saturation curve), and 0.981 (Cerd7 saturation curve in the presence of inhibitor). For transcripts quantitation, qPCR was performed in duplicate twice, starting from cDNA prepared from two independent transfections of HEK-293T cells or fibroblast cultures. For UGCG activity determination, assays were performed in duplicate twice starting from individual cell homogenates.

Acknowledgments

This paper was supported by Università dell'Insubria, Fondo Ateneo Ricerca 2020 (to MT),Mizutani Foundation for Glycosciences (Grant 210042 to MT), and Aldo Ravelli" Center for Neurotechnology and Experimental Brain Therapeutics (to MT and RP). The authors declared no conflict of interest. P.S. is employee and stockholder of Sanofi.

Abbreviations

Glycosyltransferases are named according to the HUGO recommendations. Cer, ceramide; GlcCer, glucosylceramide; Cerd7, deuterated ceramide; GlcCerd7, deuterated glucosylceramide; LC-MS/MS, liquid chromatography-tandem mass spectrometry.

References

Andersson, L.; Cinato, M.; Mardani, I.; Miljanovic, A.; Arif, M.; Koh, A.; Lindbom, M.; Laudette, M.; Bollano, E.; Omerovic, E.; Klevstig, M.; Henricsson, M.; Fogelstrand, P.; Swärd, K.; Ekstrand, M.; Levin, M.; Wikström, J.; Doran, S.; Hyötyläinen, T. et al., 2021: Glucosylceramide synthase deficiency in the heart compromises β1-adrenergic receptor trafficking. *European heart journal*., **42**, 4481–4492.

Aronica, A.; Avagliano, L.; Caretti, A.; Tosi, D.; Bulfamante, G. Pietro; Trinchera, M., 2017: Unexpected distribution of CA19.9 and other type 1 chain Lewis antigens in normal and cancer tissues of colon and pancreas: Importance of the detection method and role of glycosyltransferase regulation. *Biochimica et biophysica acta. General subjects*., **1861**, 3210–3220.

Baccam, G. C.; Xie, J.; Jin, X.; Park, H.; Wang, B.; Husson, H.; Ibraghimov-Beskrovnaya, O.; Huang, C. L., 2022: Glucosylceramide synthase inhibition protects against cardiac hypertrophy in chronic kidney disease. *Scientific Reports*., **12**, 9340.

Bataller, M.; Sánchez-García, A.; Garcia-Mayea, Y.; Mir, C.; Rodriguez, I.; LLeonart, M. E., 2021: The Role of Sphingolipids Metabolism in Cancer Drug Resistance. *Frontiers in Oncology*., **11**, 807636.

Belarbi, K.; Cuvelier, E.; Bonte, M. A.; Desplanque, M.; Gressier, B.; Devos, D.; Chartier-Harlin, M. C., 2020: Glycosphingolipids and neuroinflammation in Parkinson's disease. *Molecular Neurodegeneration*., **15**, 1–16.

Cabrera-Salazar, M. A.; DeRiso, M.; Bercury, S. D.; Li, L.; Lydon, J. T.; Weber, W.; Pande, N.; Cromwell, M. A.; Copeland, D.; Leonard, J.; Cheng, S. H.; Scheule, R. K., 2012: Systemic delivery of a glucosylceramide synthase inhibitor reduces CNS substrates and increases lifespan in a mouse model of type 2 gaucher disease. *PLoS ONE*., **7**, e43310.

Chueakwon, P.; Jatooratthawichot, P.; Talabnin, K.; Ketudat Cairns, J. R.; Talabnin, C., 2022: Inhibition of Ceramide Glycosylation Enhances Cisplatin Sensitivity in Cholangiocarcinoma by Limiting the Activation of the ERK Signaling Pathway. *Life*., **12**, 351.

Crespo, P. M.; Silvestre, D. C.; Gil, G. A.; Maccioni, H. J. F.; Daniotti, J. L.; Caputto, B. L., 2008: c-Fos activates glucosylceramide synthase and glycolipid synthesis in PC12 cells. *Journal of Biological Chemistry*., **283**, 31163–31171.

Dodge, J. C.; Tamsett, T. J.; Treleaven, C. M.; Taksir, T. V.; Piepenhagen, P.; Sardi, S. P.; Cheng, S. H.; Shihabuddin, L. S., 2022: Glucosylceramide synthase inhibition reduces ganglioside GM3 accumulation, alleviates amyloid neuropathology, and stabilizes remote contextual memory in a mouse model of Alzheimer's disease. *Alzheimer's Research and Therapy*., **14**, 19.

Fu, Z.; Yun, S. Y.; Won, J. H.; Back, M. J.; Jang, J. M.; Ha, H. C.; Lee, H. K.; Shin, I. C.; Kim, J. Y.; Kim, H. S.; Kim, D. K., 2019: Development of a Label-Free LC-MS/MS-Based Glucosylceramide Synthase Assay and Its Application to Inhibitors Screening for Ceramide-Related Diseases. *Biomolecules & therapeutics*., **27**, 193–200.

Fujii, T.; Tanaka, Y.; Oki, H.; Sato, S.; Shibata, S.; Maru, T.; Tanaka, Y.; Tanaka, M.; Onishi, T., 2021: A new brain-penetrant glucosylceramide synthase inhibitor as potential Therapeutics for Gaucher disease. *Journal of neurochemistry*., **159**, 543–553.

Hayashi, Y.; Horibata, Y.; Sakaguchi, K.; Okino, N.; Ito, M., 2005: A sensitive and reproducible assay to measure the activity of glucosylceramide synthase and lactosylceramide synthase using HPLC and fluorescent substrates. *Analytical Biochemistry*., **345**, 181–186.

Ichikawa, S.; Sakiyama, H.; Suzuki, G.; Jwa Hidari, K. I. P.; Hirabayashi, Y., 1996: Expression cloning of a cDNA for human ceramide glucosyltransferase that catalyzes the first glycosylation step of glycosphingolipid synthesis. *Proceedings of the National Academy of Sciences of the United States of America*., **93**, 4638–4643.

Indellicato, R.; Parini, R.; Domenighini, R.; Malagolini, N.; Iascone, M.; Gasperini, S.; Masera, N.; Dall'Olio, F.;

Trinchera, M., 2019: Total loss of GM3 synthase activity by a normally processed enzyme in a novel variant and in all ST3GAL5 variants reported to cause a distinct congenital disorder of glycosylation. *Glycobiology*., **29**, 229–241.

Indellicato, R.; Domenighini, R.; Malagolini, N.; Cereda, A.; Mamoli, D.; Pezzani, L.; Iascone, M.; Dall'olio, F.; Trinchera, M., 2020: A novel nonsense and inactivating variant of ST3GAL3 in two infant siblings suffering severe epilepsy and expressing circulating CA19.9. *Glycobiology*., **30**, 95–104.

Jennemann, R.; Volz, M.; Bestvater, F.; Schmidt, C.; Richter, K.; Kaden, S.; Müthing, J.; Gröne, H. J.; Sandhoff, R., 2021: Blockade of glycosphingolipid synthesis inhibits cell cycle and spheroid growth of colon cancer cells in vitro and experimental colon cancer incidence in vivo. *International Journal of Molecular Sciences*., **22**, 10539.

Madigan, J. P.; Robey, R. W.; Poprawski, J. E.; Huang, H.; Clarke, C. J.; Gottesman, M. M.; Cabot, M. C.; Rosenberg, D. W., 2020: A role for ceramide glycosylation in resistance to oxaliplatin in colorectal cancer. *Experimental Cell Research*., **388**, 111860.

Marshall, J.; Sun, Y.; Bangari, D. S.; Budman, E.; Park, H.; Nietupski, J. B.; Allaire, A.; Cromwell, M. A.; Wang, B.; Grabowski, G. A.; Leonard, J. P.; Cheng, S. H., 2016: CNS-accessible Inhibitor of Glucosylceramide Synthase for Substrate Reduction Therapy of Neuronopathic Gaucher Disease. *Molecular therapy : the journal of the American Society of Gene Therapy*., **24**, 1019–1029.

Monies, D.; Anabrees, J.; Ibrahim, N.; Elbardisy, H.; Abouelhoda, M.; Meyer, B. F.; Alkuraya, F. S., 2018: Identification of a novel lethal form of autosomal recessive ichthyosis caused by UDP-glucose ceramide glucosyltransferase deficiency. *Clinical genetics*., **93**, 1252–1253.

Morano, C.; Zulueta, A.; Caretti, A.; Roda, G.; Paroni, R.; Dei Cas, M., 2022: An Update on Sphingolipidomics : Is Something Still Missing ? Some Considerations on the Analysis of Complex Sphingolipids and Free-Sphingoid Bases in Plasma and Red Blood Cells. *Metabolites*., **12**, 450.

Peterschmitt, M. J.; Saiki, H.; Hatano, T.; Gasser, T.; Isaacson, S. H.; Gaemers, S. J. M.; Minini, P.; Saubadu, S.; Sharma, J.; Walbillic, S.; Alcalay, R. N.; Cutter, G.; Hattori, N.; Höglinger, G. U.; Marek, K.; Schapira, A. H. V.; Scherzer, C. R.; Simuni, T.; Giladi, N. et al., 2022: Safety, Pharmacokinetics, and Pharmacodynamics of Oral Venglustat in Patients with Parkinson's Disease and a GBA Mutation: Results from Part 1 of the Randomized, Double-Blinded, Placebo-Controlled MOVES-PD Trial. *Journal of Parkinson's disease*., **12**, 557–570.

Riboldi, G. M.; Di Fonzo, A. B., 2019: GBA, Gaucher disease, and parkinson's disease: From genetic to clinic to new therapeutic approaches. *Cells*., **8**, 364.

Roy, K.; Khiste, S.; Liu, Z.; Liu, Y. Y., 2019: Fluorescence HPLC Analysis of the in-vivo Activity of Glucosylceramide Synthase. *Bio-Protocol*., **9**.

Sabnis, R. W., 2022: Modified Benzofuran-carboxamide Compounds as Glucosylceramide Synthase Inhibitors for Treating Diseases. *ACS medicinal chemistry letters*., **13**, 879–880.

Salustiano, E. J.; da Costa, K. M.; Freire-De-Lima, L.; Mendonça-Previato, L.; Previato, J. O., 2020: Inhibition of glycosphingolipid biosynthesis reverts multidrug resistance by differentially modulating ABC transporters in chronic myeloid leukemias. *The Journal of biological chemistry*., **295**, 6457–6471.

Sardi, S. P.; Viel, C.; Clarke, J.; Treleaven, C. M.; Richards, A. M.; Park, H.; Olszewski, M. A.; Dodge, J. C.; Marshall, J.; Makino, E.; Wang, B.; Sidman, R. L.; Cheng, S. H.; Shihabuddin, L. S., 2017: Glucosylceramide synthase inhibition alleviates aberrations in synucleinopathy models. *Proceedings of the National Academy of Sciences of the United States of America*., **114**, 2699–2704.

Schömel, N.; Gruber, L.; Alexopoulos, S. J.; Trautmann, S.; Olzomer, E. M.; Byrne, F. L.; Hoehn, K. L.; Gurke, R.; Thomas, D.; Ferreirós, N.; Geisslinger, G.; Wegner, M. S., 2020: UGCG overexpression leads to increased glycolysis and increased oxidative phosphorylation of breast cancer cells. *Scientific Reports*., **10**, 8182.

Sidransky, E.; Nalls, M. A.; Aasly, J. O.; Aharon-Peretz, J.; Annesi, G.; Barbosa, E. R.; Bar-Shira, A.; Berg, D.;

Bras, J.; Brice, A.; Chen, C. M.; Clark, L. N.; Condroyer, C.; De Marco, E. V.; Dürr, A.; Eblan, M. J.; Fahn, S.; Farrer, M. J.; Fung, H. C. et al., 2009: Multicenter analysis of glucocerebrosidase mutations in Parkinson's disease. *The New England journal of medicine*., **361**, 1651–1661.

Tanaka, Y.; Seto, M.; Kakegawa, K.; Takami, K.; Kikuchi, F.; Yamamoto, T.; Nakamura, M.; Daini, M.; Murakami, M.; Ohashi, T.; Kasahara, T.; Wang, J.; Ikeda, Z.; Wada, Y.; Puenner, F.; Fujii, T.; Inazuka, M.; Sato, S.; Suzaki, T. et al., 2022: Discovery of Brain-Penetrant Glucosylceramide Synthase Inhibitors with a Novel Pharmacophore. *Journal of medicinal chemistry*., **65**, 4270–4290.

Viel, C.; Clarke, J.; Kayatekin, C.; Richards, A. M.; Chiang, M. S. R.; Park, H.; Wang, B.; Shihabuddin, L. S.; Sardi, S. P., 2021: Preclinical pharmacology of glucosylceramide synthase inhibitor venglustat in a GBA-related synucleinopathy model. *Scientific Reports*., **11**, 20945.

Wegner, M. S.; Gruber, L.; Mattjus, P.; Geisslinger, G.; Grösch, S., 2018a: The UDP-glucose ceramide glycosyltransferase (UGCG) and the link to multidrug resistance protein 1 (MDR1). *BMC Cancer*., **18**, 153.

Wegner, M. S.; Schömel, N.; Gruber, L.; Örtel, S. B.; Kjellberg, M. A.; Mattjus, P.; Kurz, J.; Trautmann, S.; Peng, B.; Wegner, M.; Kaulich, M.; Ahrends, R.; Geisslinger, G.; Grösch, S., 2018b: UDP-glucose ceramide glucosyltransferase activates AKT, promoted proliferation, and doxorubicin resistance in breast cancer cells. *Cellular and Molecular Life Sciences*., **75**, 3393–3410.

Zhang, F.; Zhang, H., 2021: UDP-Glucose Ceramide Glycosyltransferase Contributes to the Proliferation and Glycolysis of Cervical Cancer Cells by Regulating the PI3K/AKT Pathway. *Annals of clinical and laboratory science*., **51**, 663–669.

Zulueta, A.; Caretti, A.; Signorelli, P.; Dall'Olio, F.; Trinchera, M., 2014: Transcriptional control of the B3GALT5 gene by a retroviral promoter and methylation of distant regulatory elements. *FASEB journal : official publication of the Federation of American Societies for Experimental Biology*., **28**, 946–955.

Legends to figures

Figure 1. Characterization of UGCG activity (GlcCer synthase) assayed in vitro by LC-MS/MS using Cerd7 as acceptor. (Panel A) Expression of UGCG transcript in HEK-293T cells upon transient transfection of pCDNA3-UGCG (HEK-UGCG) and in human skin fibroblasts. (Panel B) UGCG activity measured in HEK-UGCG and in human skin fibroblasts after different time of incubation. (Panel C) UGCG activity measured in HEK-UGCG or in human fibroblasts using different amounts of homogenate protein. (Panel D) Dependence of UGCG activity expressed in HEK-UGCG on the concentration of the donor substrate UDP-Glc at fixed saturating concentration of Cerd7 (60 μM). Hanes-Woolf plot of the activity values, presented in red (secondary axis) was used for calculating kinetic constants. (Panel E) Dependence of UGCG activity expressed in HEK-UGCG on the concentration of the acceptor substrate Cerd7 at fixed saturating concentration of UDP-Glc (15 mM). Hanes-Woolf plot is as in panel D. (Panel F) Inhibition of UGCG activity expressed in HEK-UGCG by various concentrations of GZ667161. The assay was performed at fixed Cerd7 concentration (40 μM). (Panel G) Dependence of UGCG activity in HEK-UGCG on the concentration of the acceptor substrate Cerd7 in the presence of a fixed concentration (10 μM) of GZ667161 inhibitor. Hanes-Woolf plot is as in panel D.

Figure 2. Ceramide (Cerd7) enzymatic conversion to glucosylceramide (GlcCerd7) was monitored by LC-MS/MS. Comparison of GlcCerd7 (panel A) and Cerd7 (panel B) profiles obtained using HEK-UGCG and mock transfected HEK-293T cells as the enzyme source. To obtain the chromatograms, 0.4 μM Cerd7 and 40 μg (expressed as protein) of cell homogenate were incubated for 30 min.

Comparison of GlcCerd7 (panel C) and Cerd7 (panel D) profiles using HEK293-UGCG as the enzyme source and various concentrations (5-25-100 μM) of GZ667161 inhibitor in the reaction mixture. To obtain the chromatograms, 4 μM Cerd7 and 14 μg (expressed as protein) of cell homogenate were incubated for 30 min. Evaluations were performed by QTrap 3200 mass spectrometer.

Comparison of GlcCerd7 (panel E) profiles obtained using human adult and neonatal fibroblasts as the enzyme source. To obtain the chromatogram, 3 μM Cerd7 and 30 μg (expressed as protein) of cell homogenate were incubated for 20 min. Evaluation was performed by high-sensitivity QTrap 5500 instead of

QTrap 3200 mass spectrometer. The content of Cerd7 was not shown here since the concentration was above the upper limit of the high-sensitivity quadrupole.